SKB

TECHNICAL REPORT 94-02

Time evolution of dissolved oxygen and redox conditions in a HLW repository

Paul Wersin, Kastriot Spahiu, Jordi Bruno
MBT Technología Ambiental, Cerdanyola, Spain

February 1994

SVENSK KÄRNBRÄNSLEHANTERING AB
SWEDISH NUCLEAR FUEL AND WASTE MANAGEMENT CO
BOX 5864 S-102 40 STOCKHOLM
TEL. 08-665 28 00 TELEX 13108 SKB S
TELEFAX 08-661 57 19

TIME EVOLUTION OF DISSOLVED OXYGEN AND REDOX CONDITIONS IN A HLW REPOSITORY

Paul Wersin, Kastriot Spahiu, Jordi Bruno

MBT Tecnología Ambiental, Cerdanyola, Spain

February 1994

Time evolution of dissolved oxygen and redox conditions in a HLW repository

Paul Wersin, Kastriot Spahiu, and Jordi Bruno

MBT Tecnología Ambiental, Parc Tecnològic del Vallès, 08290 Cerdanyola, Spain

February 1994

Keywords: Oxygen, redox potential, near-field

Abstract

The evolution of oxygen in a HLW repository has been studied using presently available geochemical background information. The important processes affecting oxygen migration in the near-field include diffusion and oxidation of pyrite and dissolved Fe(II). The evaluation of time scales of oxygen decrease is carried out with (1) an analytical approach involving the coupling of diffusion and chemical reaction, (2) a numerical geochemical approach involving the application of a newly developped diffusion-extended version of the STEADYQL code.

Both approaches yield consistent rates of oxygen decrease and indicate that oxidation of pyrite impurities in the clay is the dominant process. The results obtained from geochemical modelling are interpreted in terms of evolution of redox conditions. Moreover, a sensitivity analysis of the major geochemical and physical parametres is performed. These results indicate that the uncertainties associated with reactive pyrite surface area impose the overall uncertainties of prediction of time scales. Thus, the obtained time of decrease to 1% of inital O_2 concentrations range between 7 and 290 years. The elapsed time at which the transition to anoxic conditions occurs is estimated to be within the same time range. Additional experimental information on redox sensitive impurities in the envisioned buffer and backfill material would further constrain the evaluated time scales.

Abstract (Swedish)

Förändringen av syrehalten i ett förvar för högaktivt avfall har studerats utifrån tillgänglig geokemisk information. De viktiga processerna som påverkar syremigration i närområdet innefattar diffusion och oxidation av pyrit och löst Fe(II). Utvärderingen av tidsskalorna för syreminskningen görs med (1) en analytisk metod som innefattar kopplingen mellan diffusion och kemisk reaktion, (2) en numerisk metod som innefattar tillämpning av en version av STEADYQL-koden som nyligen utvecklats till att innefatta även diffusion.

Båda metoderna ger samstämmiga hastigheter för syreminskning och pekar på att oxidation av pyrit i leran är den dominerande processen. De erhållna resultaten tolkas i form av utveckling av redoxförhållanden. Dessutom genomförs en känslighetsanalys av de viktigaste geokemiska och fysiska parametrarna. Dessa resultat pekar på att de osäkerheter som har att göra med reaktiv pyrityta dominerar osäkerheterna i förutsägelsen om tidsskalor. Den tid som erhålls för att minska O_2 koncentrationen till 1 % av den ursprungliga ligger mellan 7 och 290 år. Den tidpunkt då övergången till anoxiska förhållanden sker uppskattas vara inom samma tidsintervall. Mer experimentell information om redoxkänsliga föroreningar i de tilltänkta buffert- och återfyllnadsmaterialen skulle ytterligare kunna begränsa det uppskattade tidsintervallet.

Table of materials

1 Introduction

In the envisaged design for a final HLW repository highly compacted bentonite is used as a buffer material around the fuel-containing canisters in the vertically oriented placement holes (Fig. 1). A bentonite-sand mixture forms the backfill material in the tunnels. During the excavation and emplacement process, air and entrapped O_2 are introduced into the previously anoxic system. Therefore, the initial redox conditions in the near field are dominated by the presence of dissolved oxygen. This is expected to strongly affect the corrosion of potential canister materials and the mobility of possibly released radionuclides. With time the amount of dissolved O_2 in the bentonite medium will decrease through (1) diffusion into the surrounding rock and (2) via chemical reactions and thus ultimately anoxic conditions will be established. The quantification of this temporal decrease of O_2 is a prerequisite part of adequate safety analysis.

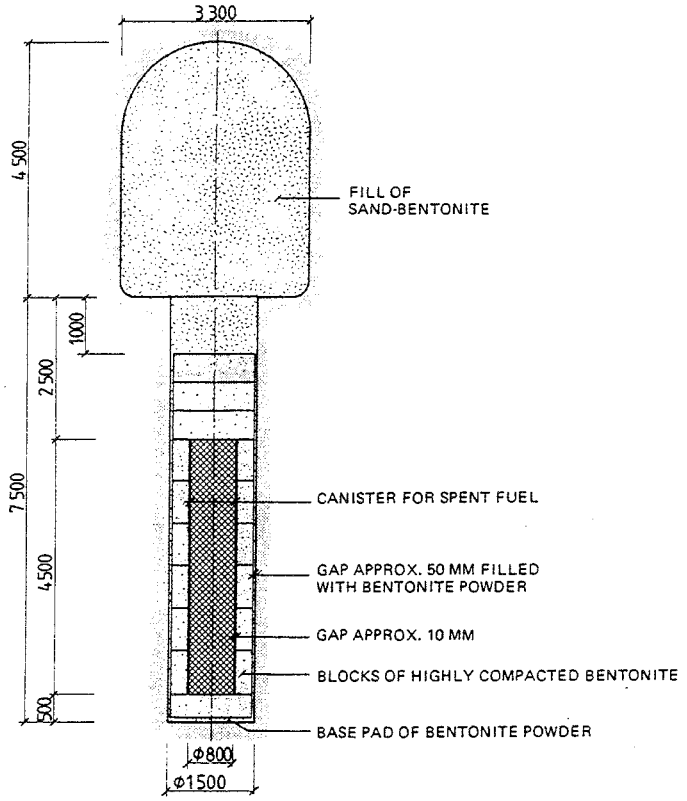

Figure 1. Waste emplacement geometry of Swedish HLW repository (dimensions given in mm). Taken from SKB 91.

The migration of O_2 in the bentonite medium toward the surrounding rock is primarily controlled by diffusion and reaction with reducing compounds, i.e. electron donors (e.g., Neretnieks, 1986). Potential electron donors in the bentonite medium mainly include impurities such as pyrite and organic carbon (Van Olphen and Fripiat, 1979). Other possible reactants with O_2 in the near field are the metallic canister material (Cu and/or Fe) and dissolved Fe(II) which may diffuse from the outside rock. The relative importance of each individual process depends on the geochemical boundary conditions, physical properties of the bentonite, and the reaction kinetics. The former two problems have been investigated in previous SKB work and are reasonably well understood. Thus, a recent study (Wanner et al., 1992) has established the major chemical relationships for bentonite porewater on the basis of experimental data (Werme, 1988). Experimental studies involving diffusion of dissolved gases, such as methane or hydrogen in compacted bentonite (Neretnieks and Skagius, 1978; Neretnieks, 1985) have indicated relatively consistent diffusivities. The kinetics of oxygen consumption with respect to near field modelling have not been investigated in detail. Neretnieks (1983) performed some rough estimations on the amount of O_2 reacting with the surrounding rock and the canister. Spahiu and Bruno (1992) have recently emphasized the importance of pyrite oxidation for oxygen removal in the bentonite. Their estimations are based on kinetic information of pyrite oxidation in carbonate-buffered solutions (Nicholson et al., 1988).

The purpose of this work is to quantify the decrease of dissolved oxygen with time under conditions relevant in the near field. This will involve six steps:

Step 1: Presentation of a conceptual model and evaluation of kinetic data by extending our previous work (Spahiu and Bruno, 1992).

Step 2: Analytical approach to the coupled diffusion/reaction process.

Step 3: Numerical geochemical approach: Adaptation of the geochemical STEADYQL code (Furrer et al., 1989) to transient conditions (steady-state approach for a series of consecutive boundary conditions).

Step 4: Comparison of results obtained by both approaches.

Step 5: Assessment of redox conditions and sensitivity analysis with aid of STEADYQL.

Step 6: Estimation of realistic time scales of O_2 depletion and oxic/anoxic transition.

2 Description of the problem

2.1 Conceptual model

The depletion of dissolved O_2 in the bentonite buffer material is controlled by the kinetics of oxidation reactions and by diffusion. The main processes are schematically illustrated in Fig. 2. Diffusion processes are denoted with F, where F_1 and F_2 present O_2 diffusive fluxes perpendicular and parallel to the emplacement cylinder, respectively. F_3 presents the net flux between the cylinder and the overlying tunnel. Chemical reaction processes, denoted R, occur within the buffer and backfill material. In this section we will perform an initial evaluation of the relative importance of each process and establish the appropriate simplifications and constraints for the subsequent quantitative assessment.

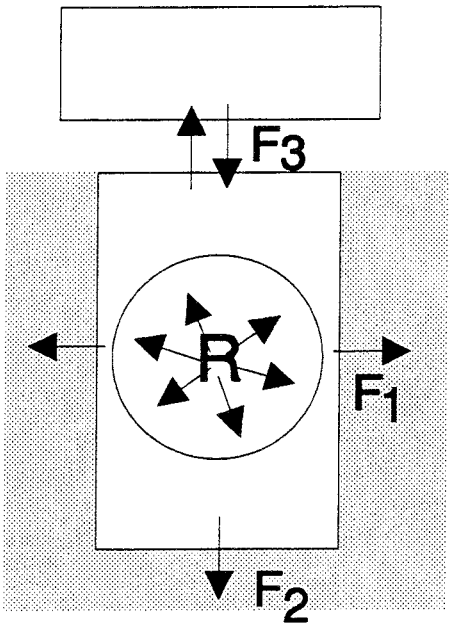

Figure 2. Schematic presentation of fluxes of O_2 in a repository. R: chemical reactions; F_1, F_2, F_3: diffusion.

2.2 Chemical reactions

2.2.1 Pyrite

Wyoming bentonite contains pyrite impurities of around 0.2 to 0.3 % (Grauer, 1986; Van

Olphen and Fripiat, 1979). Pyrite surfaces show high sensitivity toward electron acceptors and react with dissolved O_2 to Fe(III) oxyhydroxides and sulfate (Singer and Stumm, 1970; Nordstrom, 1982) according to:

$$FeS_2 + {}^{15}/_4 O_2 + {}^7/_2 H_2O \text{ --->} Fe(OH)_3 + 2SO_4^{2-} + 4H^+ \qquad (1)$$

The reaction kinetics have been studied relatively extensively under acidic (McKibben and Barnes, 1986), neutral and alkaline conditions (Moses and Herman, 1991; Nicholson et al., 1988; 1990). It could be shown that O_2 concentration, pyrite surface area, concentration of dissolved Fe(III), temperature, and the presence of bacteria affect the rate of pyrite oxidation (Lowson, 1982). Of particular interest for performance assessment is the experimental data of Nicholson et al. (1988; 1990) who followed pyrite oxidation in carbonate-buffered solutions at 3-60°C over long time periods (up to 14 months). Their oxidation rates showed a linear dependence on exposed surface area and O_2 concentration, and an Arrhenius dependence with regard to temperature. A simple shrinking core model (Levenspiel, 1972) was used to describe the long-term kinetic data.

We have used the data of Nicholson et al. (1988; 1990) and the shrinking core model to extrapolate kinetics of pyrite oxidation to near field conditions. First, this requires an estimation of the maximum Fe(III) oxyhydroxide overlayer thickness. We assume spherical pyrite particles of the order of 5-100 μm diameter, d, and estimate the surface areas from the relationship $S = 6/(\rho d)$ where ρ is the particle density (4.4 g/cm^3). The particle size of sulfides encountered in marine sedimentary environments is of similar order or lower (1-100 μm) (Berner, 1971). Taking 0.2 % pyrite in bentonite (Grauer, 1986; Van Olphen and Fripiat, 1979), a dry density of 1.7 g/cm^3 and a porosity of 0.38 for compacted bentonite, a surface area of 0.24- 0.012 m^2 pyrite per liter of porewater is calculated. The maximum amount of $Fe(OH)_3$ as overlayer formed is obtained from the total amount of available O_2 (10 mg/dm^3) according to Eq. 1. Taking 2.7 g/cm^3 as density for amorphous Fe(III) oxyhydroxide one obtains a maximum surface layer thickness of 0.26-0.013 μm. This calculation indicates that less than 1% of the mole fraction of pyrite has reacted upon total depletion of oxygen. Moreover, the thickness of the overlayer will not affect the kinetics significantly, which simplifies the kinetic approach associated with the shrinking core model. Therefore, a first overall reaction rate can be assumed to hold for reaction (1) (cf. Nicholson et al., 1988).
Specifically, it allows to express the long-term reaction rate of reaction (1) as:

$$-\frac{dC}{dt} = k\,C \qquad (2)$$

where C is conc. of dissolved O_2.

The second step involves the estimation of the reaction rate constant. In that case we have calculated the time elapsed to consume all the oxygen in the repository for various particle sizes in the range 5-100 μm, with a low concentration of oxygen (0.05%), according to the procedure outlined in Spahiu and Bruno (1992). The time calculated ranges from 8.5-306 years for the range of particle sizes considered here. In order to get conservative estimates of rate constants, this time was assumed equal to the time elapsed to lower the concentration of oxygen from the initial one to 0.05%, with a first order reaction rate. Inserting these times to the solution of Eq. (2), the rate constants were calculated.
Finally, for the range of particle sizes, we obtain a range of first-order reaction rate constants of $2.2 \cdot 10^{-8}$ - $6.2 \cdot 10^{-10}$ s^{-1}. As a reference case we will use $3 \cdot 10^{-9}$.

2.2.2 Other Fe(II) compounds

The oxidation of ferrous iron leads to precipitation of ferric oxyhydroxide:

$$Fe^{2+} + {}^{1}/_{4}O_2 + {}^{5}/_{2}H_2O \text{ ----> } Fe(OH)_3(s) + 2H^+ \qquad (3)$$

The kinetics of this reaction is well established (Stumm and Lee, 1961) with a rate law in the form of:

$$-\frac{dFe(II)}{dt} = k\,[O_2(aq)][H^+]^{-2}[Fe(II)] \qquad (4)$$

with $k\ (20\ °C) = 5 \cdot 10^{-14}$ mol dm^{-3} s^{-1}

Under oxidizing conditions there is no dissolved Fe(II) initially. However, dissolved Fe(II) slowly diffuses from the surrounding anoxic medium. Furthermore, Fe(II) impurities other than pyrite, such as Fe(II)-bearing silicates (mainly biotite) or siderite may occur to a small extent in bentonite (Grauer, 1986). The overall rate of oxidation of biotite is orders of magnitude slower than the one of pyrite (White and Yee, 1985; Malmström al. 1993) and therefore the influence of Fe(II) silicates is not taken into account in this study. Oxidation of siderite in air and water is relatively fast (Wersin, 1990). The amount of siderite impurities in Wyoming bentonite has so far, to the authors' knowledge, not been reported. Therefore, in order to be conservative in the assessment of O_2 consumption, we neglect the possible influence of siderite oxidation.

2.2.3 Canister material

In the current Swedish design of a HLW repository (SKB 1991), copper is selected as canister

material. Under oxidizing conditions the copper canister is expected to oxidize to soluble Cu(II) (e.g., SKB 1991):

$$Cu^{\circ} + {}^{1}/_{2}O_2 + 2H^{+} \text{---> } Cu^{2+} + H_2O$$

The flux of O_2 diffusing to the canister surface is low compared to the one diffusing to reactive surface areas of impurities. Thus, taking our estimation of the reactive pyrite surface area (Section 2.2.1), less than 1% of the O_2 flux is expected to react with the copper surface compared to the one reacting with pyrite. Therefore, canister corrosion will not significantly affect oxygen consumption. On the other hand, the corrosion kinetics will be strongly affected depending on the O_2 concentrations. Therefore, and this is a important point of this study, the determination of the time scales of consumption is critical for appropriate estimation of canister corrosion.

2.2.4 Organic carbon

Besides sulfide, ferrous iron, and the metallic copper canister potential reactants of O_2 in the bentonite medium includes organic carbon. Although there would be sufficient carbon to reduce all the initially present O_2

$$CH_2O + O_2 \text{----> } HCO_3^{-} + H^{+}$$

the process is limited by the low reactivity of the organic C. It is known that refractory organic C has been preserved for millions of years in bentonite in spite of exposure to air (cf. Vogt and Köster, 1978).

In summary, as a first conservative approximation, the pyrite oxidation reaction can be assumed to dominate the overall reaction of O_2 in the bentonite.

2.3 Diffusion

The transport of oxygen in bentonite is controlled by the diffusive flux, F which depends on the concentration gradient $c - c_x$ according to Fick's first law:

$$F = - \frac{D\,(c - c_x)}{\Delta x}$$

where D is the diffusion coefficient and Δx is the diffusion distance. Due to the cylindrical geometry of the repository (Fig. 2) two directions of O_2 fluxes (F_1 and F_2) out of the

bentonite into the surrounding rock are expected. Furthermore, a flux (F_3) from the overlying tunnel filled with bentonite/sand should be considered (Neretnieks, 1983).

The diffusivity of dissolved O_2 in compacted clay has not been measured. We have estimated it from measurements (Neretnieks and Skagius, 1978) made on methane in compacted bentonite (~2000 m^3/kg) which showed a 100 times decrease of D with regard to the molecular diffusivity in water. Hence, for O_2 we estimate $D = 1.25\ 10^{-11}\ m^2/s$.

The change of O_2 concentration with time due to diffusion follows Fick's second law:

$$\frac{\partial C}{\partial t} = D \frac{\partial^2 C}{\partial x^2}$$

The quantification of the total O_2 evolution requires a mathematical assessment of a combination of diffusion and chemical reaction process and to determine the relative contribution of each process. This is outlined in the following section.

3 Analytical assessment of coupled diffusion/reaction

3.1 Boundary conditions and dimensional analysis

The decrease of O_2 over time following a coupled diffusion/reaction is expressed in the one-dimensional form as:

$$\frac{\partial C}{\partial t} = D \frac{\partial^2 C}{\partial x^2} + R$$

where R stands for chemical reaction. R can be approximated by a reaction of first-order kinetics as shown in Section 2. Thus,

$$\frac{\partial C}{\partial t} = D \frac{\partial^2 C}{\partial x^2} - k C \qquad (5)$$

We assess this equation for the vertical cylinder (Fig. 1) neglecting at this point the possible contribution of the tunnel. In order to evaluate the relative contribution of diffusion and reaction we set boundary conditions for the point displaying the longest diffusion distance which is situated in the centre, just on top of the canister (Fig. 1). The boundary conditions for this

point are:

$$C_{(x,\,0)} = C_0$$

and $$C_{(0,\,t)} = 0$$

The second boundary condition arises from the fact that, outside of the bentonite, all O_2 diffuses much faster (cf. Neretnieks, 1983). Furthermore, there is no O_2 transfer through the copper canister wall:

$$\frac{\partial C_{(l,\,t)}}{\partial x} = 0$$

where l is the diffusion distance (2.5 m). In order to deduce which factor dominates O_2 consumption, Eq. (5) is transformed in dimensionless form as follows:
By introducing the dimensionless variables

$$y = \frac{C}{C_0} \text{ and } z = \frac{x}{l}$$

we get $$\frac{\partial y}{\partial t} = \left(\frac{D}{l^2}\right)\cdot\left(\frac{\partial^2 y}{\partial z^2}\right) - k\,y$$

Dividing both sides by D/l^2 we obtain:

$$\frac{\partial y}{\partial\left(\frac{D\,t}{l^2}\right)} = \frac{\partial^2 y}{\partial z^2} - \left(\frac{k\,l^2}{D}\right) y$$

This equation contains the following dimensionless numbers:

- The Fourier number : $Fo = \frac{D\,t}{l^2}$

- The Damköhler number: $Da = \frac{k\,l^2}{D}$

Finally, the dimensionless form of Eq. 1 can be written:

$$\frac{\partial y}{\partial Fo} = \frac{\partial^2 y}{\partial z^2} - Da\,y \qquad (6)$$

The Damköhler number is a measure of the relative importance of the chemical reaction as compared to diffusion in the oxygen consumption. For values $Da \geq 10$ oxygen consumption is dominated by the chemical reaction and the influence of diffusion can be neglected. On the other hand diffusion will dominate for $0 \leq Da \leq 1$, while both diffusion and chemical reaction should be considered for values of Da = 1 - 10 (Villermaux, 1982).
In the case of a point situated on top of the copper canister, where the distance of diffusion is longest, we have a value of the Damköhler number (calculated with $k = 3 \cdot 10^{-9}$ s^{-1}, cf. previous section):

$$Da = \frac{(3 \cdot 10^{-9} \cdot 2.5^2)}{1.25 \cdot 10^{-11}} = 1500$$

This very high value of the Damköhler number shows that diffusion is negligibly slow as compared to the chemical reaction and does not practically influence the oxygen consumption. Mathematically, for $Da >>> \partial^2 y/\partial z^2$ Eq. 6 gives:

$$\frac{\partial y}{\partial Fo} = - Da\, y$$

which is in fact Eq. 2, that is $dC/dt = -k\, C$.

3.2 Discussion

Compared to the case of diffusion parallel to the cylinder walls discussed above, lateral diffusion (with l = 0.35 m) is more significant for the assessment of O_2 decrease rates. Fig. 3 illustrates the resulting Damköhler numbers obtained for the range of kinetic constants of pyrite oxidation (cf. section 2.2.1). This shows that diffusion still only has minor influence on the consumption of oxygen and that the rate can be described approximately by Eq. 2.

A further point to consider is the migration of O_2 in the overlying tunnel containing a bentonite-sand mixture. A similar calculation as performed for the cylinder shows that oxygen is predominantly consumed by chemical reaction. Furthermore, it is evident from the large difference in diffusion resistance (Neretnieks, 1983), that the amount of available O_2 transported to the rock is much higher than the one to the cylinder. Therefore, the diffusive flux from the tunnel to the cylinder (F_3 in Fig. 2) can be considered negligible.

The conclusion that can be drawn from the analytical approach outlined here is that the decrease of dissolved O_2 in the cylinder can be approximated by a simple first-order reaction (Eq. 2). The rate of decrease is illustrated in Fig. 4 for the range of reaction rate constants

estimated for pyrite oxidation in bentonite. This shows that the rate critically depends on the size of the particles.

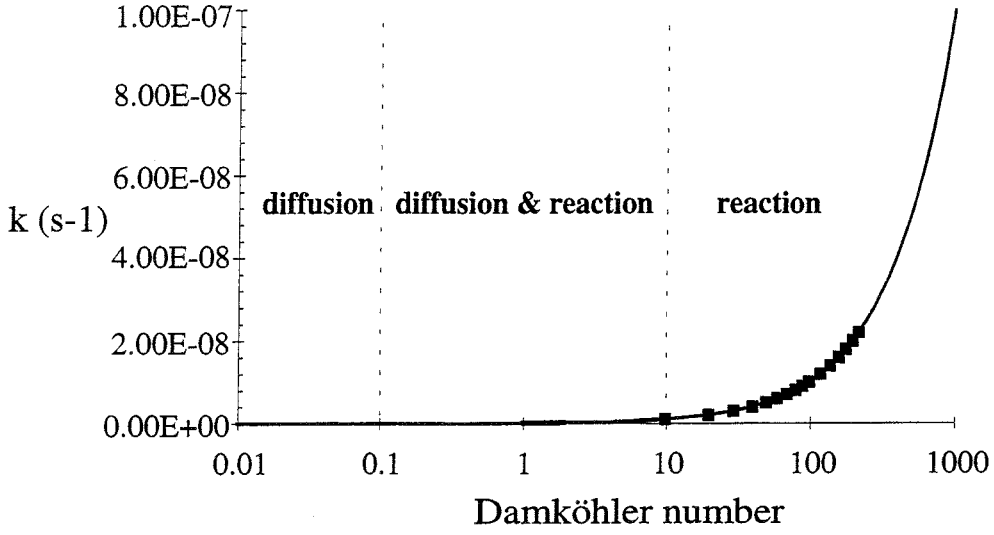

Figure 3. Coupled diffusion and first-order reaction. The relationship between the rate constant and the Damköhler number (a measure for the rate-controlling process) is shown. Squares: Range expected for oxygen migration in the buffer material (see text).

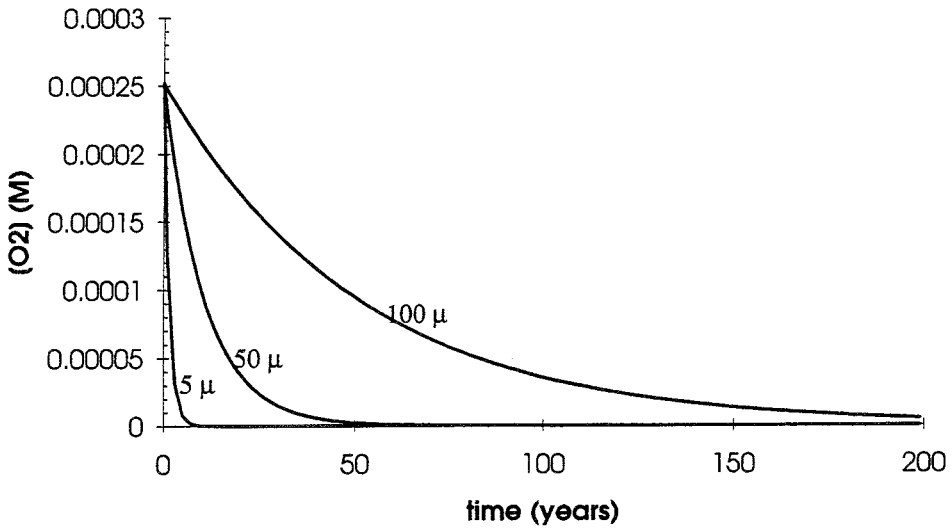

Figure 4. Rate of O_2 decrease after enclosure assuming first-order kinetics for pyrite oxidation for three different particle sizes (µ ≡ micrometer).

4 Geochemical modelling with the STEADYQL approach

4.1 Introduction

In addition to the analytical analysis of O_2 evolution, we have applied a numerical approach to the problem, on the basis of the programme STEADYQL. The STEADYQL code, developed by Furrer and co-workers (Furrer et al., 1989), is a kinetic geochemical model which includes fast (equilibrium-driven) and slow (kinetically-driven) processes and is based on the steady-state condition. The STEADYQL algorithm solves for mass action equations, flux balance, and mole balance at steady-state. The usefulness of STEADYQL lies in the (1) simple presentation of a great variety of geochemical situations, (2) identification the relative importance of the chemical processes involved, (3) straightforward determination of fluxes, (4) an analytical sensitivity analysis.

In the recently developed diffusion-extended version of STEADYQL (Furrer and Wehrli, 1992) chemical processes between two limiting boundary boxes, from which dissolved constituents diffuse in and out, are modelled (Fig. 5).

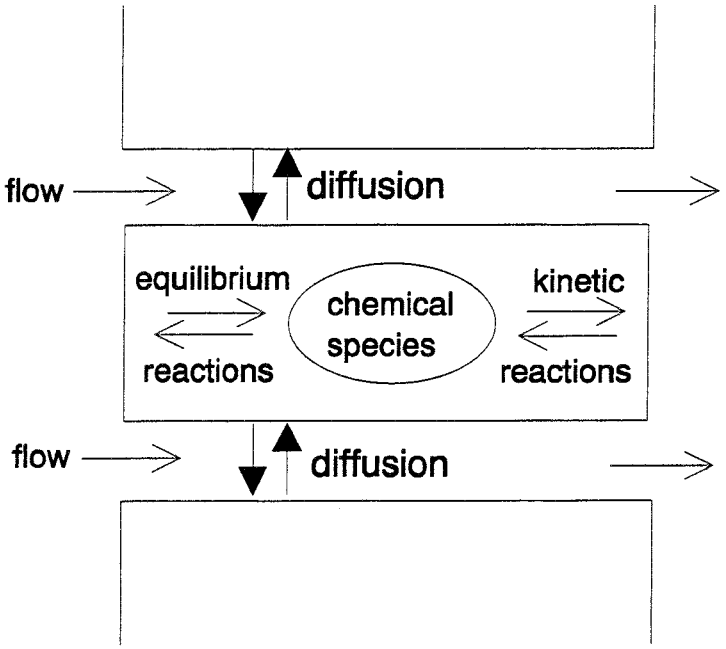

Figure 5. Schematic presentation of diffusion-extended STEADYQL. The two limiting boxes present pools with fixed compositions from where dissolved species diffuse in and out towards the central box. Here, equilibrium reactions, kinetic reactions, and diffusion occur simultaneously (partly after Furrer and Wehrli, 1992).

This approach is useful when the dominant transport process is diffusion rather than flow or when both processes are important. It allows to quantify the relative contribution of each slow process (kinetic reactions, diffusion) for the overall flux of a given component under the assumption of the steady-state condition. The diffusion-extended version has been applied to redox transformations in a lacustrine system (Furrer and Wehrli, 1992) and to canister corrosion in bentonite clay (Wersin et al., 1993a and 1993b).

4.2 Application of the STEADYQL approach to oxygen evolution

4.2.1 Presentation of modelling procedure

The decrease of O_2 in bentonite using STEADYQL is assessed by a step-wise procedure. First, under the assumption of steady-state, the geochemical boundary conditions are constrained for time zero and the first calculation is performed. This yields the relative fluxes of O_2 for diffusion and chemical reaction. Thereof, the net amount of O_2 consumed for a given time interval is calculated. The decreased amount of total O_2 after this time interval is computed, a new steady-state condition is assumed, and the second STEADYQL calculation is performed. This procedure is repeated until the original concentration of oxygen has decreased to about 1%. The total procedure can thus be called a consecutive steady-state approximation. In the following we will outline this approach in detail, present the results, and compare them to the analytical one, described in Section 3.

4.2.2 Geochemical constraints at steady-state

The geochemical description of the bentonite medium with regard to oxygen evolution is assessed on the basis of the equilibrium model for bentonite (Wanner et al., 1992) and the kinetics elaborated in section 2.2. After the selection of the necessary components, species, and kinetic reactions, these are integrated into STEADYQL as fast and slow process.

Fast processes: These include equilibrium reactions between the components H^+, Fe^{2+}, CO_3^{2-}, Ca^{2+}, SO_4^{2-}, HS^- and O_2 whereof O_2 does not form any other species. The resulting chemical species are expressed by the stoichiometry of the reaction and the corresponding formation constants. For the bentonite medium, we have used the total concentrations, as given for reference bentonite porewater (Wanner et al., 1992). Furthermore, we have imposed equilibrium with respect to calcite following the equilibrium model of Wanner et al. (1992). For the medium occurring in the surrounding granitic rock, we have taken the composition of Allard

water (Standard Swedish type groundwater) (Allard et al., 1983). Table 1 gives the selected components and corresponding total concentrations which we have used for our calculations. The speciation calculations for the bentonite and the granitic water compositions are performed with the MICROQL code (Westall, 1986) which displays the same format as STEADYQL and therefore data from output files are easily transferred.

Table 1 Total concentrations (M) and pH of bentonite and rock porewaters used for STEADYQL calculations.

	bentonite	rock
pH	9.0	8.1
CO_3^{2-}	5.0E-03	1.9E-03
Fe^{2+}	1.0E-10	5.0E-06
Ca^{2+}	1.0E-04	4.6E-04
SO_4^{2-}	1.0E-03	1.0E-04
HS^-	1.9E-09	1.0E-09
O_2	2.5E-04	1.0E-10

Slow processes: The relevant slow processes include (1) kinetic oxidation reactions and (2) diffusion of each species in and out of the limiting boxes as imposed by the diffusion-extended version of STEADYQL (cf. Fig. 6). The diffusive flux F of each species i is presented as two rate equations according to Fick's first law:

$$F_i = d_{(i,1)} C_{(x,i)} - d_{(i,2)}$$

where $d_{(i,1)} = \frac{D_i}{\Delta x}$ and $d_{(i,2)} = \frac{D_i C_{(0,i)}}{\Delta x}$

or $$F_{(i,1)} = d_{(i,1)} C_{(x,i)} \quad (7)$$

and $$F_{(i,2)} = d_{(i,2)} \quad (8)$$

Δx is the diffusion distance, $C_{(0,i)}$ and $C_{(x,i)}$ is the concentration of species i at distance zero and x from bentonite cylinder wall, respectively. The units of F are typically mol m^{-2} s^{-1}. Since we are interested in the content of dissolved O_2, we rather express fluxes per unit volume (mol dm^{-3} s^{-1}). The diffusion coefficients D in the compacted clay for each dissolved

species have been estimated from the corresponding diffusivities in water (Applin and Lasaga, 1984; Wehrli, 1993) and assuming a constant relative decrease of a factor of 100 (cf. Neretnieks and Skagius, 1978).

The potentially relevant oxidation processes in the oxic bentonite have been elucidated in section 2.2. They include oxidation of pyrite and oxidation of dissolved Fe(II). The flux of O_2 consumed per unit volume (R_1) corresponding to pyrite oxidation is (Eq. 1).

$$R_1 = s_1 k_1 [O_2(aq)] \tag{9}$$

s_1 is the stoichiometric coefficient of the reaction, equal to $^{15}/_4$ and k_1 is the first-order reaction constant ($2.2 \cdot 10^{-8}$ - $6.2 \cdot 10^{-10}$ s^{-1}). As a reference case we take the mean value $3 \cdot 10^{-9}$ s^{-1} as we have done for the analytical approach in section 3. The flux of O_2 corresponding to Fe(II) oxidation (see Eq. 3) is

$$R_2 = s_2 k_2 [Fe(II)]_{tot} [H^+]^{-2} [O_2(aq)] \tag{10}$$

s_2 is equal to $^1/_4$ and k_2 is $5.0 \cdot 10^{-14}$ mol dm^{-3} s^{-1}. The total flux of O_2 consumed through chemical reactions is $R = R_1 + R_2$.

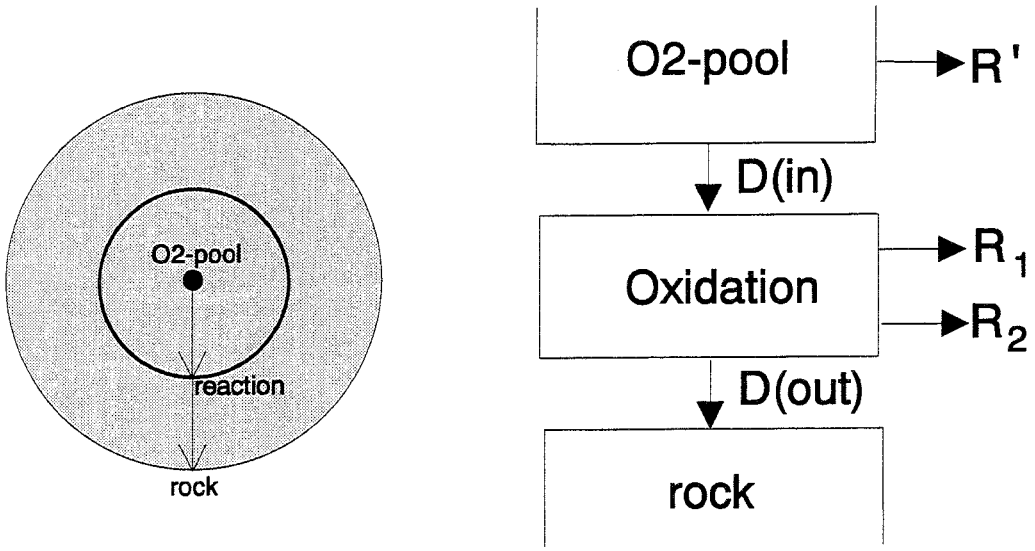

Figure 6. Schematic presentation of modelling concept. Diffusive fluxes of O_2 in the clay medium are viewed as influx from an imaginary central pool ($J_{D(in)}$) and an efflux into the rock ($J_{D(out)}$). In the central box oxidation of pyrite (R_1) and of dissolved Fe(II) (R_2) affect diffusive fluxes. The geometric boundary conditions which are implied in the model are shown on the left sketch.

4.2.3 Approximation of the coupled diffusion/reaction processes

After defining the general geochemical constraints of the system we define the initial boundary conditions for O_2 using the diffusion-extended STEADYQL programme which is designed as a multi-box model. We assign the two limiting boxes to the surrounding rock and the oxygen box, respectively. Thus, the O_2-box represents the pool of oxygen in the bentonite. The "diffusion" box between the two limiting boxes, represents the O_2-consuming reactions within the bentonite. In other words, the flux of O_2 is viewed as deriving from a point source located at the center of the cylinder, from where it diffuses out, reacts at mid-distance, and diffuses into the rock (Fig. 6). It should be noted, however that this simplified concept lacks one important factor, namely the reaction of O_2 in the center which occurs simultaneously with diffusion. Therefore, reaction in the limiting O_2-box is also taken into account as shown in Fig. 6 where the O_2 fluxes are illustrated in and between the boxes. Fig. 6 also depicts the geometrical relationships used in our description of the problem. This allows to constrain the diffusion process and to quantify the "reaction" constants d_1 and d_2 for O_2 (see Eqs. 7 and 8). Taking a diffusivity of $\sim 1.25\ 10^{-11}$ m^2/s in compacted bentonite (cf. Neretnieks and Skagius, 1978) and a diffusion distance of 0.35 m between the reaction box and both limiting boxes (Fig. 6): $d_1 = 8.57\ 10^{-11}$ m/s. The value of d_2 which characterizes the diffusive flux back into the limiting boxes differs significantly for both boxes. The back diffusion into O_2 box will be constrained by C_0, which in this case is the concentration of O_2 in the limiting O_2-box. On the other hand the diffusion out of the rock-box is very low in view of the anoxic conditions therein.

Having defined all the fast and slow processes and corresponding constants, the STEADYQL calculation yields the steady-state solution for this coupled diffusion/reaction process. Thus, the calculated composition in the intermediate "diffusion" box represents the porewater at steady-state. Moreover, fluxes derived from each slow process are obtained for each component. Since we are primarily interested in the consumption of O_2, we will view the obtained O_2 fluxes in order to deduce the net flux, J_{0_2}, per volume out of the bentonite medium. The steady-state condition imposes that the sum of all fluxes is zero. Referring to the notation used in Fig. 6, this means that

$$J_{D(in)} = J_{D(out)} - R \qquad (11)$$

where $J_{D(in)}$ is the net diffusive flux out of the O_2-box, $J_{D(out)}$ is the net diffusive flux into of the rock-box, and R is the sum of fluxes arising from O_2-consumption reactions in the intermediate box. However, as pointed out above, there exists a further source of O_2 consumption, the chemical reactions of O_2 within the O_2-box, denoted R'. This flux is not taken into ac-

count by the present version of STEADYQL but must be included for the evaluation of O_2 over time. As a rough approximation we set $R' \approx R$ and derive the net flux J of O_2 out of the bentonite medium (chemical reactions and diffusion) to be:

$$J_{O_2} \approx J_{D(in)} + R \qquad (12)$$

4.2.4 Oxygen decrease with time

Since the total O_2 concentration changes with time, it follows a transient behaviour and can be represented by a series of steady-state situations. We approximate this problem with STEADYQL by calculating the net decrease of O_2 after a given short time interval $\Delta t = 0.25$ years. Thus, taking $C_{t=0} = C_0$, then

$$C_{\Delta t} = C_0 - \frac{J_{\Delta t}}{\Delta t}$$

This gives a new boundary condition, with a slightly lower concentration gradient between the limiting O_2 box ($C = C_{\Delta t}$) and rock-box ($C \approx 0$). The calculation is repeated and a new net decrease of O_2 after Δt obtained with $C_{2\Delta t}$ for time $2\Delta t$. This process is repeated for n time intervals Δt until $C_{n\Delta t} \approx 0.001 \cdot C_0$.

4.3 Results

In this section we first present the results obtained for the reference case as discussed in Section 4.2. These are compared to the results obtained from the analytical approach. Finally, we perform a sensitivity analysis of the important parameters.

4.3.1 O_2 fluxes

Steady-state fluxes for O_2 are illustrated for three different O_2 source concentrations in Fig. 7. These present situations of (1) an early stage of O_2 conditions ($[O_2(aq)] = 10^{-4}$ M) in the clay, (2) an intermediate stage ($[O_2(aq)] = 10^{-5}$ M), and (3) an advanced stage of O_2 consumption ($[O_2(aq)] = 10^{-6}$ M), respectively. The visualization of the obtained fluxes, shown as influx and efflux is aided by comparing with Fig. 6 where the concept is presented. The results indicate for all cases that fluxes of reaction (R_1 and R_2) dominate the overall efflux of O_2.

The dominant reaction in the overall consumption is pyrite oxidation which consumes >90% of the available O_2. This is very consistent with the result obtained from the analytical solution of coupled diffusion/reaction for a closed system in a transient regime and thus supports

our modelling concept.

The usefulness of the STEADYQL approach is also manifested by the fact that a number of kinetic processes can be studied without further mathematical complications. Thus, the simultaneous oxidation of Fe(II) which diffuses from the anoxic granitic medium into the bentonite can be quantified. As discussed in Section 2.2 the kinetics of Fe(II) oxidation are very fast and clearly diffusion controlled above pH 8 (Stumm and Lee, 1961), i.e. the diffusion flux of Fe(II) or O_2, depending on the conditions, controls the rate. At initial conditions, the flux of Fe(II) is small compared to the overall O_2-flux and therefore the amount of O_2 consumed is negligible (cf. Fig. 7, time 1). On the other hand, the influence of dissolved Fe(II) becomes considerable at evolved stages of O_2 consumption. Fig. 7 (time 3) indicates that almost all of the efflux of O_2 derives from Fe(II) oxidation when the total O_2 concentration has decreased to 0.5% of the initial content.

4.3.2 O_2 evolution with time

The application of the consecutive steady-state approximation outlined in section 4.2.4 yields an estimate of the decrease of dissolved oxygen in the clay with time. Fig. 8 shows this result for the reference case and compares it with the simple analytical approximation derived for the closed clay system (see section 3), which is a first-order reaction. The STEADYQL approximation shows a slightly slower decrease compared to the analytical one, but, in general, a good agreement between the two approaches is observed. This similarity is somewhat unexpected because both modelling concepts differ significantly. This result suggests that the approximation used with aid of STEADYQL yields quantitative estimates on time scales of chemical transformations. Moreover, the uncertainty introduced by representing the problem with a relatively simple box-model is much lower than the one associated with the kinetics of pyrite oxidation.

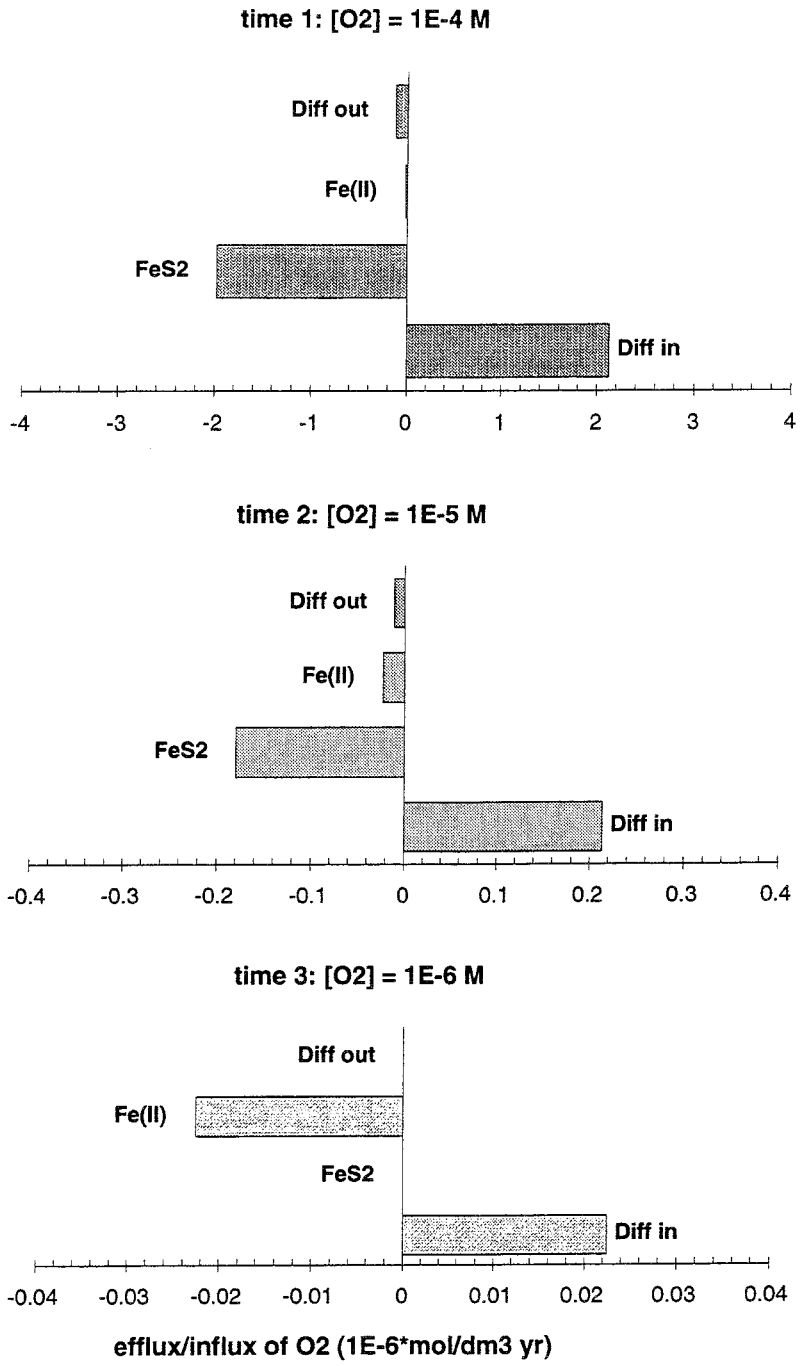

Figure 7. Fluxes of O_2 obtained from STEADYQL results for three different concentrations of oxygen. Note that in all cases >90% of the efflux is produced by oxidation processes.

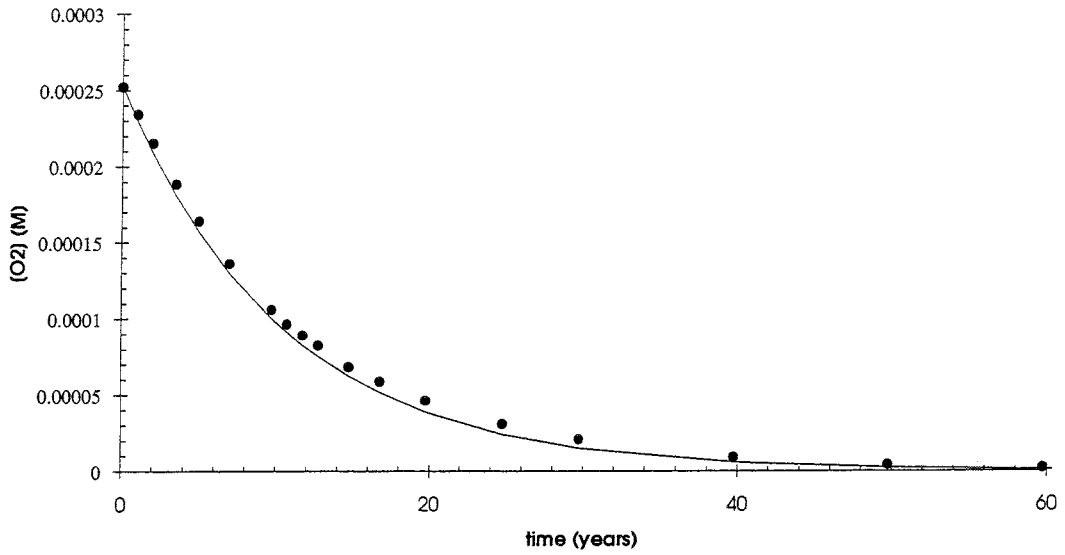

Figure 8. Decrease rates of O_2 calculated for the "reference case" (see text). Lower line: Analytical approach ($C = C_0\, e^{-kt}$). Circles: STEADYQL approach (consecutive steady-state approximation).

4.3.3 Effect of O_2 decrease on redox potential

The redox potential E_H is affected by the same processes that induce oxygen decrease. Thus, the change in redox potential in the clay is controlled by the major oxidation processes which include oxidation of pyrite and dissolved Fe(II). During the initial stages of the repository oxidizing conditions are imposed by the abundance of dissolved O_2. E_H should therefore be controlled by oxygen fugacity ($\approx p_{O_2}$) according to the equilibrium

$$O_2(g) + 4H^+ + 4e^- \Leftrightarrow 2H_2O \qquad (13)$$

$$\text{where } E_H = E_0 + \frac{RT}{4F} (\log p_{O_2} - 4pH) \qquad (14)$$

and $\log K = 83.11$

E_0 is the standard redox potential for O_2/H_2O (1.23 V), R is the gas constant, T the temperature, and F the Faraday constant. The pH value in the clay is assumed to be around 9. In our calculations we have, so far, neglected the effect of temperature and assumed 25 °C, which gives $^{RT}/_{F} \approx 0.059$ V. Field measurements in oxidizing environments have shown that the measured E_H is usually lower than the one calculated from measured O_2 and Eq. 14 (Stumm and Morgan, 1981). Here, we use this redox equilibrium as an upper limit for the calculation

of E_H. At high p_{O_2}, the flux of dissolved Fe(II) entering from the surrounding anoxic medium and reacting with O_2 is consumed by precipitation of Fe(III) and does not influence E_H. However, during later stages, the O_2 content will have decreased to an extent that the influence of Fe(II) on E_H becomes notable. This effect is enhanced by the distinct chemical behaviour of the oxidants involved. Whereas the redox equilibria involving O_2 are sluggish due to kinetic effects, especially at low p_{O_2}, the Fe(III)/Fe(II) equilibrium reactions are rapid and, within the time range considered here, can be regarded as instantaneous. Therefore, we assume that, as soon as dissolved Fe(II) increases in the clay, the redox potential is controlled by the Fe^{2+}/Fe^{3+} redox couple. Using the results obtained by the steady-state approximation, the relationship between $[O_2(aq)]$ and $[Fe^{2+}]$ as a function of time can be established and the time scale for the onset of Fe^{2+}/Fe^{3+} control estimated as illustrated in Fig. 9 (upper 2 graphs). For this equilibrium the redox potential is defined as

$$E_H = E_0 + \frac{R\,T}{F} \log \left(\frac{[Fe^{3+}]}{[Fe^{2+}]}\right) \qquad (15)$$

with $E_0 = 0.77$ V. The activity of Fe^{3+} in the clay is controlled by Fe(III) oxyhydroxide solubility:

$$Fe(OH)_3 + 3H^+ \Leftrightarrow Fe^{3+} + 3H_2O \qquad (16)$$

The solubility constant for Fe(III) oxyhydroxide shows a relatively broad range and depends principally on the crystallinity of mineral. Thus, ferrihydrite is almost six orders of magnitude more soluble than goethite. Field redox measurements performed in deep groundwaters (Grenthe et al. 1992; Banwart et al., 1993) indicated that the redox potential was controlled by the $Fe^{2+}/Fe(OH)_3$ equilibrium. Thereof, Grenthe et al. (1992) suggested a solubility constant $K_s^* = -0.4 \pm 2.6$ for Eq. 16, which is significantly lower than the widely accepted value of ferrihydrite (Langmuir, 1969) with $K_s^* = 4.89$. Due to the uncertainties involved in predicting the solubility of Fe(III) in the clay, we assume a conservative range and take these two values as solubility limits. Thus, $-0.4 < K_s^* < 4.89$. Inserting K_s^* and rearranging Eq. 15, we obtain:

$$E_H = E_0^* - \frac{R\,T}{F} (\log[Fe^{2+}] + 3pH) \qquad (17)$$

where $E_0^* = 0.77 + \frac{RT}{F} \log K_s^*$

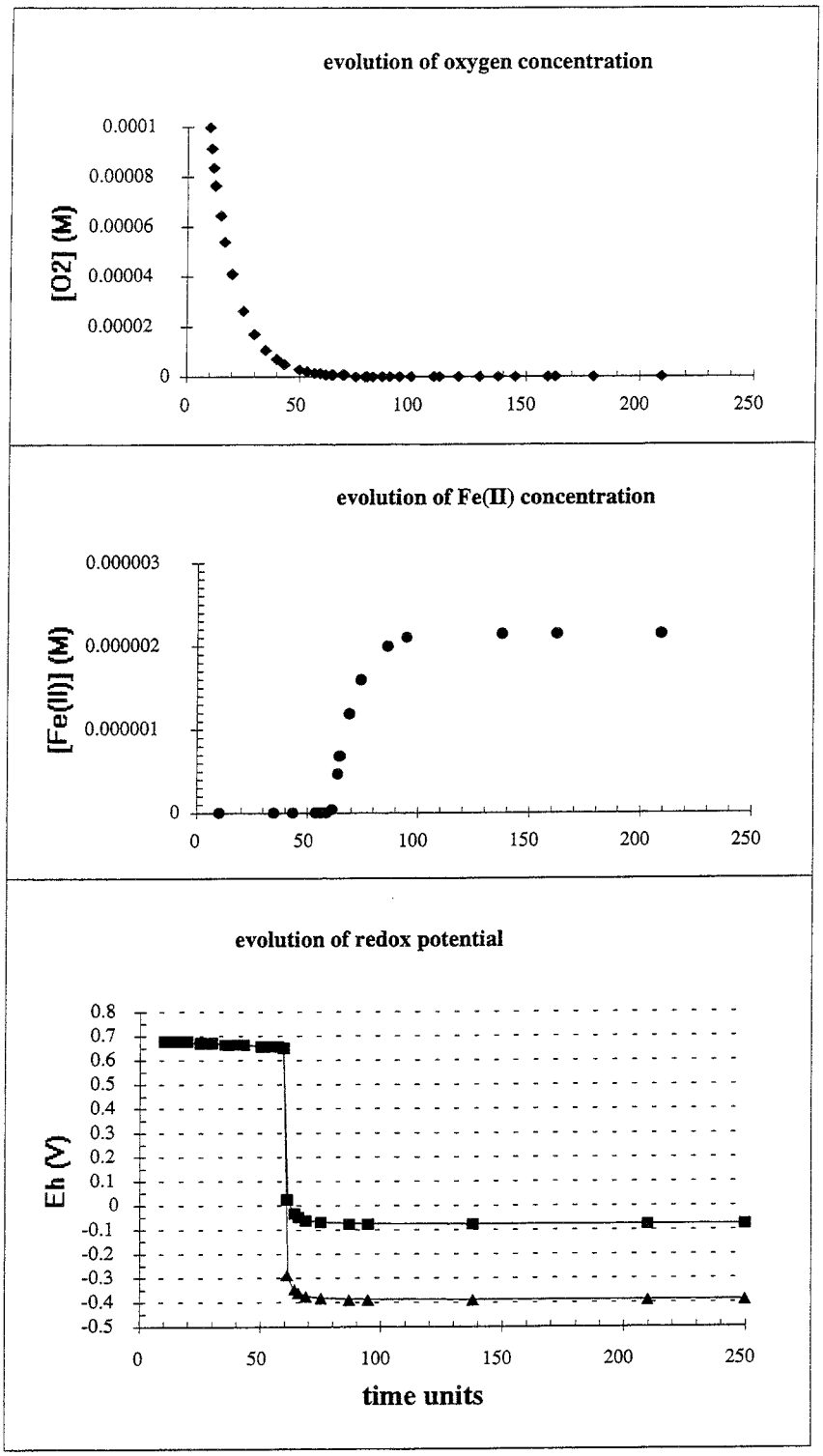

Figure 9. STEADYQL results showing concurrent evolution of O_2 and Fe(II) (upper two graphs) and redox potential (lower graph). Time units correspond to years assuming the reference case situation (see text). The squares show E_H results obtained assuming ferrihydrite equilibrium. The triangles represent E_H values obtained from an intermediate solubility constant of Fe(III)oxide which has been determined in anoxic granitic groundwaters by Grenthe et al. (1992).

The activity of Fe^{2+} in the clay is derived (Grenthe et al., 1992) from the relationship between $Fe(II)_{tot}$ and its carbonate complexes, $FeCO_3(aq)$, $Fe(CO_3)_2^{2-}$ and their corresponding constants (Bruno et al., 1992).

$$[Fe^{2+}] = \frac{Fe(II)_{tot}}{(1+\beta_1^{-1}[CO_3^{2-}]+\beta_2^{-1}[CO_3^{2-}]^2)} \quad (18)$$

where $\beta_1 = 5.5$ and $\beta_2 = 7.1$ at zero ionic strength.

The calculated E_H for the corresponding p_{O_2} and $[Fe^{2+}]$, respectively (Eqs. 14 and 17) as a function of time is illustrated in Fig. 9 (lower graph). The strong shift to lower potentials reflects the increase of Fe(II) in the clay as a result of O_2 depletion. Note that the redox potentials are very sensitive to the imposed Fe(III) oxyhydroxide solubilities. Thus, the upper solubility limit gives rise to E_H values of ≈ -0.08 V whereas the lower one yields values of ≈ -0.39 V (Fig. 9).

4.3.4 Sensitivity analysis

Here we assess the sensitivity of the potentially important geochemical and physical parameters and derive the relative change of O_2 consumption and of the redox potential in the clay compared to the reference case discussed above. In Fig. 10 (upper graph) the elapsed time of initial O_2 decrease to 1% is plotted as a function of the relative change with respect to the reference case. Fig. 10 (lower graph) illustrates the elapsed time for reaching Fe^{2+}/Fe^{3+} redox equilibrium for the same cases.

pH: The variation of pH to higher or lower values (pH 10 and 8) does not affect the resulting fluxes of O_2 noticeably and therefore the uncertainty of the pH in the clay can be neglected for the present purpose. The concentration of carbonate is dependent on the imposed pH and calcite equilibrium and therefore, equally as pH, does not affect O_2 fluxes.

Fe(II): The flux of Fe(II) from the granitic medium strongly affects the O_2 fluxes and the redox potential once O_2 levels have decreased to a a similar range as the resulting Fe(II) concentration in the clay. In the reference case we have taken $5 \cdot 10^{-6}$ M $Fe(II)_{tot}$ in the granitic medium which is a conservative estimate, since it presents a low value compared to ones measured in anoxic groundwaters. For example, concentrations observed in the Finnsjön area range between $5 \cdot 10^{-6}$ - $1.6 \cdot 10^{-4}$ M (cf. SKB 91, Table 5-3). The increase of diffusive flux of Fe(II) results in increase of O_2 consumption. As shown in Fig. 10 the effect on both O_2 consumption and E_H is considerable. At [Fe(II)] $>10^{-5}$ M an enhanced decrease is observed. The calcula-

tions performed with the upper value ($1.6 \cdot 10^{-4}$ M) indicate that the rate of O_2 decrease is enhanced once the P_{O_2} level has reached ~ 75% of the initial (0.2 atm). The effect of Fe(II) flux on the redox potential is more pronounced. The decrease of E_H to negative potentials, assuming the upper [Fe(II)] limit, occurs about three times faster relative to the reference case.

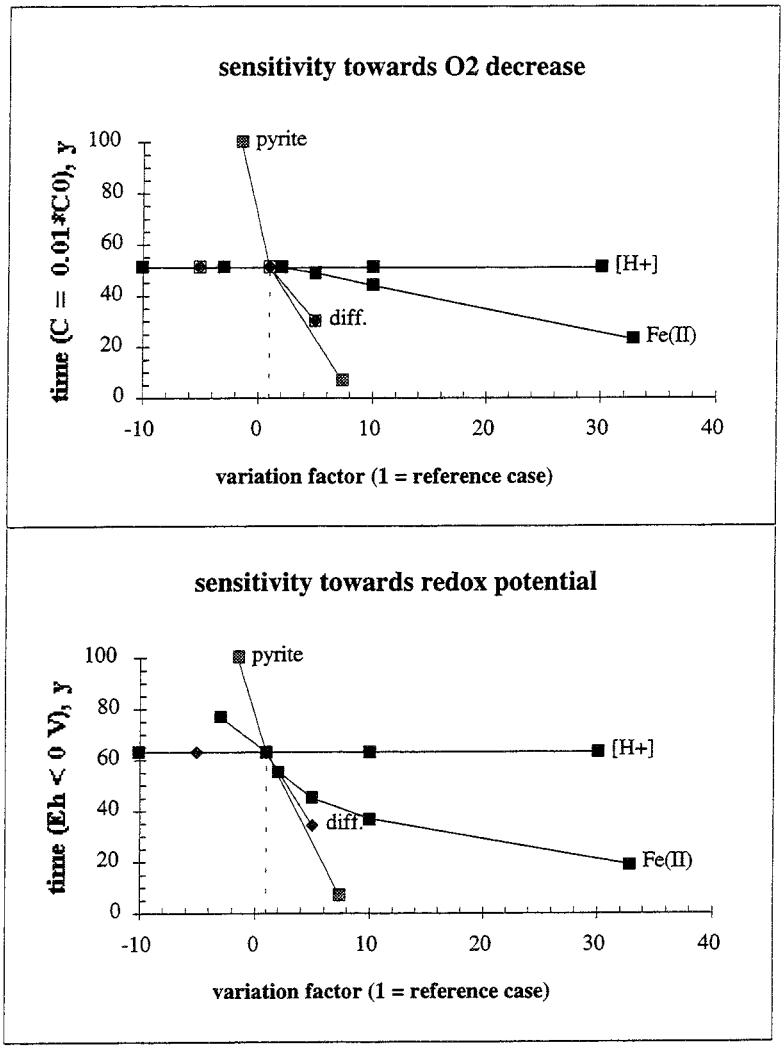

Figure 10. Summary of sensitivity analysis by varying various important parameters in the STEADYQL model. Dashed line refers to "reference case". The upper graph shows the elapsed time in years of initial O_2 decrease to 1% as a function of the relative change with respect to the reference case. The lower graph illustrates the elapsed time of oxic ---> anoxic transition.

It is also noteworthy to point out that the increase in [Fe(II)] in the clay is limited by the formation of secondary Fe(II) minerals. The mineral expected to control Fe(II) solubility under these conditions is siderite (Bruno et al., 1992; Banwart et al., 1993). Assuming siderite equi-

librium as the upper limit of Fe^{2+} reached in the bentonite, the E_H calculated by Eq. (7) and (8) is -0.1V and -0.41V, respectively, depending on the Fe(III) solubility constant used. This is only slightly lower than obtained from STEADYQL results.

Pyrite kinetics: The uncertainty in kinetic rate constants is outlined in section 2.2.1. It is determined by the uncertainty regarding the reactive surface area of pyrite in the compacted bentonite; i.e., the surface "seen" by the porewater. Since our results indicate that pyrite oxidation is the dominant O_2 consumption process, the estimated range of first-order rate constants ($2.2 \cdot 10^{-8}$ - $6.2 \cdot 10^{-10}$ s^{-1}) in the clay give rise to the largest variations in prediction of time scales. This is illustrated in Fig. 10 where the STEADYQL calculations indicate a resulting time range of roughly 7 - 290 years for both O_2 decrease to 1% and for establishing anoxic conditions.

Diffusion coefficients: The range of uncertainties for pore diffusivities in compacted bentonite is taken to be a factor of ~ 10 which we estimated on the basis of the compilation given by Brandberg and Skagius (1991). A decrease of D by factor of five with respect to the reference case does not have any notable difference on the half life of O_2 or the evolution of E_H because O_2 consumption is controlled by chemical reaction in the clay. An increase of D results in a higher diffusive flux and a higher proportion of diffusion out to the rock. Thus, an increase of D leads to a higher overall efflux of O_2. STEADYQL calculations indicate that a five-fold increase in D results in a decreased half-life of O_2 by a factor of about two.

5 Time scales

5.1 Synthesis of the data

Both modelling approaches used to derive the decrease of O_2 as a function of time yield a consistent results in terms of time scales. Moreover, the results indicate that pyrite oxidation largely controls O_2 decrease which can be described approximately by first-order kinetics depending on $[O_2(aq)]$ and particle size. The rate of O_2 decrease is illustrated in Fig. 4 which shows the range of rates obtained. Thus, the time of decrease to 1% of initial O_2 concentrations ranges from 7 to 290 years. The evolution of the redox potential is derived indirectly from the fluxes of dissolved Fe(II) and the resulting concentration of Fe^{2+} in the clay, as calculated by the consecutive steady-state approximation. The underlying assumption, which is based on chemical arguments and geochemical observations, is that the E_H is controlled by $Fe(OH)_3/Fe^{2+}$ equilibrium rather than by p_{O_2}, once Fe(II) increases in the system. Since Fe(II)

and O_2 evolution in the clay are intimately coupled, the evolution of E_H largely depends on the rate of O_2 decrease. In other words, the kinetics of pyrite oxidation also largely affect the transition from oxic to anoxic conditions. In addition, the Fe(II) content in the surrounding medium influences E_H. However, the effect of [Fe(II)] variation in the groundwater is relatively small compared to the one induced by uncertainties in pyrite surface areas (cf. Fig. 10). The time scales of oxic/anoxic transition are summarized in Fig. 11.

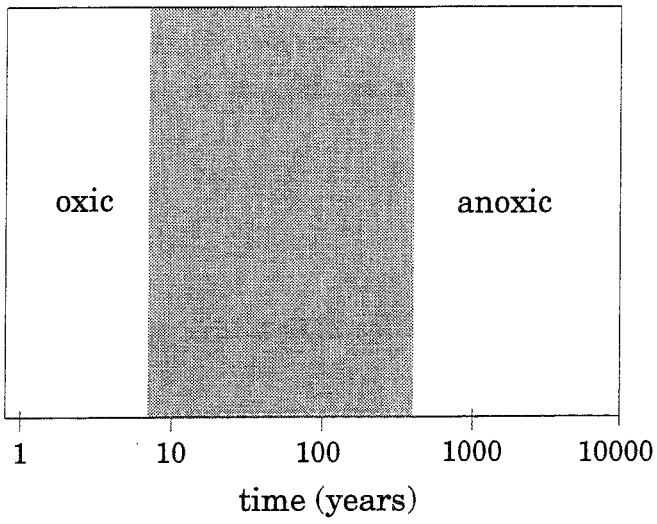

Figure 11. Range of time scales (shaded area) for oxic---->anoxic transition as calculated from uncertainty associated with pyrite surface area in the bentonite which strongly affects oxidation kinetics.

5.2 Uncertainties

Major uncertainties in prediction of time scales arise, as outlined above, in the uncertainties associated with pyrite oxidation kinetics in the bentonite medium. These, in turn, mainly are due to the missing experimental information regarding grain size and reactive surface area in the clay. The uncertainty of the O_2 diffusivity is comparatively small and does not significantly influence the results. This also holds for the uncertainties with regard to important geochemical variables in the clay-granite system, such as pH, alkalinity, [Fe(II)] which do not significantly influence time scales.

All calculations have been performed assuming Standard State conditions. The effect of increased temperature (50-60°C vs. 25°C) on O_2 evolution can only be qualitatively estimated in view of the presently available experimental information. The kinetic data of Nicholson et al. (1988) on pyrite oxidation indicate an increase of the rate by a factor of ~10 at 60°C relative to 25°C. This suggests that O_2 is consumed significantly faster at higher temperatures.

The initial amount of dissolved O_2 has also been evaluated at Standard State from water-air equilibrium to be 2.5 10^{-4} M. Increase in temperature to 60°C decreases O_2-solubility, but increase in pressure due to the overburden (~ 50 bar) increases O_2 solubility such that all the available O_2 can dissolve in the porewater (Neretnieks, 1983). The resulting calculated concentration of O_2(aq) is about 2.7 10^{-4} M which is only slightly higher than one applied to the calculations. From these considerations we expect the combined influence of increased temperature and pressure to enhance the kinetics relative to Standard State conditions considered here. Therefore, the predictions elaborated here are on the conservative side. The effect of ionic strength (which was not taken into account) can be neglected in view of the comparatively low concentrations involved.

5.3 Implications

In spite of significant uncertainties of estimated time scales some useful implications for near-field predictions can be established.

1) The decrease of oxygen in the near-field takes place at a relatively fast rate. Thus, at time scales lower than 300 years, oxygen will have decreased to the levels expected in the surrounding anoxic granite. The redox conditions in the clay will shift to negative potentials during this time period.

2) Pyrite impurities in the clay are reactive electron donors. These redox sensitive surfaces provide an efficient trap for oxygen. Their reactivity is not expected to be altered after reaction with oxygen due to the excess of available surface area. Thus, pyrite surfaces are also expected to contribute to the immobilization of redox sensitive radionuclides, such as U, Tc, Np.

3) Canister corrosion at high oxidation potentials (>100 mV) will occur for relatively short time periods. From our results, corrosion at low oxidation potentials (-100 to -400 mV) will prevail after 10-300 years of emplacement.

4) Pretreatment of the bentonite is not recommended because it may passivate the natural redox sensitive surfaces.

5) Further experimental information on pyrite impurities in terms of surface area and reaction kinetics will allow a more accurate prediction of oxygen and E_H evolution.

6 Summary and conclusions

In this work we have studied the evolution of dissolved oxygen in the near-field on the basis of available experimental information on kinetics and transport in the bentonite backfill. Firstly, the relevant kinetic processes which consume oxygen are reviewed in the light of their relative importance at near-field conditions. Secondly, an analytical approach to coupled diffusion/reaction is performed to quantify the contribution of each process. Thirdly, a recently developed geochemical model based on steady-state (STEADYQL) is applied to (a) verify the results obtained by the analytical approach, (b) assess the geochemical sensitivity of the system, (c) evaluate the evolution of the redox conditions.

Both approaches used yield consistent results in terms of the overall rate of oxygen decrease. Moreover, they indicate that oxidation of pyrite impurities in the clay is the dominant process ($\geq$ 90% of overall rate). Calculations performed with STEADYQL enable to predict the evolution of redox equilibria involving the Fe^{3+}/Fe^{2+} couple. This allows to estimate the time scale of the oxic/anoxic transition within the bentonite system. In the modelling procedure, first a reference case is considered which takes into account appropriate estimates of the physical and geochemical parameters. Thus, it assumes realistic porewater compositions, realistic diffusivities expected in compacted bentonite, and an intermediate reaction rate constant for pyrite oxidation. Thereafter, a sensitivity analysis is performed which evaluates the effect of the important variables on O_2 and E_H and determines the uncertainties of time scales.

The results of the sensitivity analysis indicate that the uncertainty associated with pyrite oxidation kinetics dominates the overall uncertainties of time scale predictions. Thus, the obtained time of decrease to 1% of initial O_2 concentrations range between 7 and 290 years. The elapsed time at which the transition to anoxic conditions occurs is estimated to be within the same time scale.

Based on the obtained results some useful implications can be drawn. Pyrite impurities constitute an important pool of reactive electron donors. Their reactivity is not expected to be significantly affected by their interaction with dissolved oxygen and therefore they may also serve as "trap" for redox sensitive radionuclides, such as U, Np, and Tc. Further experimental data on redox sensitive impurities in bentonite are required in order to constrain predictions of redox conditions in the near-field.

7 Acknowledgments

We would like to express our thanks to Dr. Geri Furrer (ETH Zürich) and Dr. Eduard Plasari (Université de Nancy) whose comments have helped to improve this report. We also thank Dr. Bernhard Wehrli (ETH Zürich) for providing information on diffusion coefficients.

8 References

Allard B., Larson S.A., Tullborg E.-L., Wikberg P. (1983). Chemistry of deep groundwaters from granitic bedrock. KBS TR 83-59.

Applin and Lasaga (1984). Geochim. Cosmochim. Acta 48, 2151.

Banwart S., Gustafsson E., Laaksoharju M., Nilsson A.-C., Tullborg E.-L., and Waltin B. (1993). Redox processes in a granitic coastal aquifer. Wat. Res. Res. (submitted).

Berner R.A. (1971). Principles of sedimentology. McGraw Hill.

Brandberg F. and Skagius K. (1991). Porosity, sorption, and diffusivity data compiled for the SKB 91 study. SKB TR 91-16.

Bruno J., Wersin P., and Stumm W. (1992). On the influence of carbonate in mineral dissolution: II. The solubility of $FeCO_3$(s) at 25°C and 1 atm total pressure. Geochim. Cosmochim. Acta 56, 1149-1155.

Furrer G. and Wehrli B. (1992). Biogeochemical processes at the sediment-water interface: Measurements and modeling. Appl. Geochem. Suppl. No. 2, 117-119.

Furrer G., Westall J., Sollins P. (1989). The study of soil chemistry through quasi-steady-state models: I. Mathematical definition of model. Geochim. Cosmochim. Acta 53, 595-601.

Furrer G., Westall J., Sollins P. (1990). The study of soil chemistry through quasi-steady-state models: II. Acidity of soil solutions. Geochim. Cosmochim. Acta 54, 2363-2374.

Grauer R. (1986) Bentonite as a backfill material in the high-level waste repository: chemical aspects. Nagra NTB 86-12E.

Grenthe I., Stumm W., Laaksoharju M., Nilsson A.-C., Wikberg P. (1982). Redox potentials and redox reactions in deep groundwater systems. Chem. Geol. 98, 131-150.

Hallberg R.O., Östlund P., Wadsten T. (1988). Inferences from a corrosion study of a bronze cannon, applied to high level nuclear waste disposal. Appl. Geochem. 3, 273-280.

Langmuir D. (1969) The Gibbs free energies of substances in the system Fe-O_2-H_2O-CO_2 at 25°C. USGS Prof. Paper 650-B, 180-183.

Levenspiel O. (1972). Chemical reaction engineering. Wiley, New York.

Lowson R.T. (1982). Aqueous oxidation of pyrite by molecular oxygen. Chem Rev. 82, 461-497.

Malmström M., Banwart S., Duro L., and Bruno J. (1993) Kinetics of biotite dissolution at 25 °C. In: Fourth International Conference on the Chemistry and Migration Behavior of the Actinides and Fission Products in the Geosphere, Charleston, SC USA December 12-16, Abstracts, p. 14.

McKibben M.A. and Barnes H.L. (1986). Oxidation of pyrite in low temperature acidic solutions: Rate laws and surface textures. Geochim. Cosmochim. Acta 50, 1509-1520.

Moses C.O. and Herman J.S. (1991). Pyrite oxidation at circumneutral pH. Geochim. Cosmochim. Acta 55, 471-482.

Neretnieks I. (1983) Approximate calculation of what happens with oxygen that is entrapped in the repository at the time of its closure. In Corrosion resistance of a copper canister for spent nuclear fuel. The Swedish Corrosion Research Institute and its reference group. Appendix 4, pp. 39-45.

Neretnieks I. (1985). Diffusivities of some constituents in compacted wet bentonite clay and the impact on radionuclide migration in the buffer. Nucl. Technol. 71, 458-470.

Neretnieks I. (1986). Some uses for natural analogues in assessing the function of a HLW repository. Chem. Geol. 55, 175-188.

Neretnieks I. and Skagius C. (1978). Diffusivitetsmätningar av metan och väte i vat lera. KBS TR 86.

Nicholson R.V., Gilham R.W., Reardon E.J. (1988). Pyrite oxidation in carbonate-buffered solution: 1. Experimental kinetics. Geochim. Cosmochim. Acta 52, 1077-1085.

Nicholson R.V., Gilham R.W., Reardon E.J. (1990). Pyrite oxidation in carbonate-buffered solution: 2. Rate control by oxide coatings. Geochim. Cosmochim. Acta 54, 395-402.

Nordstrom D.K. (1982). Aqueous pyrite oxidation and the consequent formation of secondary iron minerals. In Acid Sulphate Weathering (ed. D.K. Nordstrom), pp. 37-56. Soil Sci. Soc. Amer., Spec. Publ. No. 10.

Olphen Van H. and Fripiat J.J. (1979). Data handbook for clay minerals and other non-metallic compounds. Pergamon Press, New York.

Singer P.C. and Stumm W. (1970) Acidic mine drainage: The rate-determining step. Science 167, 1121-1123.

SKB 91(1992). Final disposal of spent nuclear fuel. Importance of the bedrock for safety. SKB TR 92-20.

Spahiu K. and Bruno J. (1992). Pyrite oxidation in carbonate-buffered solutions. In L. Werme, P. Sellin, and N. Kjelbert. Copper canisters for nuclear high-level waste disposal. Corrosion aspects. SKB TR 92-26. Appendix, pp. 22-25.

Stumm W. and Lee G.F. (1961). Oxygenation of ferrous iron. Ind. Eng. Chem. 53, 143-146.

Stumm and Morgan (1981). Aquatic chemistry. 2nd edition. Wiley, New York.

Villermaux J. (1982). Génie de la réaction chimique. Conception et fonctionnement des réacteurs. Lavoisier, Paris.

Vogt K. and Köster H.M. (1978). Zur Mineralogie, Kristallchemie und Geochemie einiger Montmorillonite aus Bentoniten. Clay Minerals 13, 25-43.

Wanner H., Wersin P., and Sierro N. (1992). Thermodynamic modelling of bentonite-groundwater interaction and implications for near field chemistry in a repository for spent fuel. SKB TR 92-37.

Wehrli B. (1993). Pers. communication.

Werme L. (1988) (unpubl.). Cited in Wanner et al. (1992).

Wersin P. (1990). The Fe(II)-CO_2-H_2O system in anoxic natural waters: Equilibria and surface chemistry. Ph.D. dissertation. ETH Zürich.

Wersin P., Bruno J., and Spahiu K. (1993a). Kinetic modelling of bentonite-canister interaction. Implications for Cu, Fe, and Pb corrosion in a respository for spent nuclear fuel. SKB TR 93-16.

Wersin et al. (1993b). In preparation.

Westall J.C. (1986). MICROQL. A chemical equilibrium program in BASIC. Version 2 for PCs. Report 86-02, Dept. of Chemistry, Oregon State University, Corvallis, OR, 44p.

White A.F. and Yee A. (1985) Aqueous oxidation-reduction kinetics associated with coupled electron cation transfer from iron-containing silicates at 25°C. Geochim. Cosmochim. Acta 49, 1263-1275.

List of SKB reports

Annual Reports

1977-78
TR 121
KBS Technical Reports 1 – 120
Summaries
Stockholm, May 1979

1979
TR 79-28
The KBS Annual Report 1979
KBS Technical Reports 79-01 – 79-27
Summaries
Stockholm, March 1980

1980
TR 80-26
The KBS Annual Report 1980
KBS Technical Reports 80-01 – 80-25
Summaries
Stockholm, March 1981

1981
TR 81-17
The KBS Annual Report 1981
KBS Technical Reports 81-01 – 81-16
Summaries
Stockholm, April 1982

1982
TR 82-28
The KBS Annual Report 1982
KBS Technical Reports 82-01 – 82-27
Summaries
Stockholm, July 1983

1983
TR 83-77
The KBS Annual Report 1983
KBS Technical Reports 83-01 – 83-76
Summaries
Stockholm, June 1984

1984
TR 85-01
Annual Research and Development Report 1984
Including Summaries of Technical Reports Issued during 1984. (Technical Reports 84-01 – 84-19)
Stockholm, June 1985

1985
TR 85-20
Annual Research and Development Report 1985
Including Summaries of Technical Reports Issued during 1985. (Technical Reports 85-01 – 85-19)
Stockholm, May 1986

1986
TR 86-31
SKB Annual Report 1986
Including Summaries of Technical Reports Issued during 1986
Stockholm, May 1987

1987
TR 87-33
SKB Annual Report 1987
Including Summaries of Technical Reports Issued during 1987
Stockholm, May 1988

1988
TR 88-32
SKB Annual Report 1988
Including Summaries of Technical Reports Issued during 1988
Stockholm, May 1989

1989
TR 89-40
SKB Annual Report 1989
Including Summaries of Technical Reports Issued during 1989
Stockholm, May 1990

1990
TR 90-46
SKB Annual Report 1990
Including Summaries of Technical Reports Issued during 1990
Stockholm, May 1991

1991
TR 91-64
SKB Annual Report 1991
Including Summaries of Technical Reports Issued during 1991
Stockholm, April 1992

1992
TR 92-46
SKB Annual Report 1992
Including Summaries of Technical Reports Issued during 1992
Stockholm, May 1993

Technical Reports
List of SKB Technical Reports 1994

TR 94-01

Anaerobic oxidation of carbon steel in granitic groundwaters: A review of the relevant literature

N Platts, D J Blackwood, C C Naish
AEA Technology, UK

February 1994